A homogenized finite element analysis of the deformation of axially-loaded thin-walled epoxy/coir fibre-reinforced aluminum 6063 composite tubes

*B.O. Malomo

Department of Mechanical Engineering, Obafemi Awolowo University, Ile-Ife, Nigeria

bobmalom@oauife.edu.ng

Abstract. Metal-fibre hybridization is strategic to the development of efficient lightweight energy absorbing structures. In this study, the deformation of variable coir-fibre reinforcement volumes (10%-90%) hybridized at reinforcement thicknesses (10T, 15T and 20T) with aluminum alloy 6063 tubes was investigated from a continuum standpoint to unravel the underlying mechanisms of the composite's performance potential. A representative volume element (RVE) was developed to determine the effective properties of coir-fibers based on Mori-Tanaka/Benveniste theoretical model in DIGIMAT 2017.0, while the aluminum alloy properties were defined by Johnson-Cook's plasticity. Finite element (FE) simulations were implemented in ABAQUS Explicit Dynamics by deformable continuum elements to capture the damage initiation and evolution response based on the Hashin's stiffness degradation failure criteria and the strength-based cohesive zone, traction-separation law. Incidental high peaks and unstable buckling loads at the onset of crushing was significant for 10T and 15T tubes with 10-30% and 80-90% reinforcement concentrations (V_f) relative to the low frequency of fluctuations at 40-70%, V_f. Axisymmetric to non-asymmetric transformations occurred with relative significance for the tubes as the resistance to global bending increased with reinforcement thickness. The interaction between the tube walls and reinforcement layers in preventing the formation of complete folds notably increased with 15T and 20T tubes at 60% fiber concentration, where the extensional collapse by progressive delamination of the 20T tubes improved the buckling resistance at densification. In agreement with FE simulations, experimental stress-strain plots at 60% V_f, confirmed that 20T tubes indicated wider plateau region of stable crushing to underscore observed high capacities for energy absorption.

1. Introduction

As one of the most compelling performance metrics in the automotive industry to achieve a much-required competitive edge is enhanced occupant safety, automakers have continued to deploy scientific novelties that advance superior crashworthiness through the incorporation of effective structural mechanisms in state-of-the-art material forms geared towards mitigating catastrophic effects from crash conditions. In recent times, a flurry of research efforts has intensified its focus on optimizing the energy absorption efficiencies of advanced structures evolving from the profound pioneering work of Weirzbicki and Abramowicz, [1] who jointly postulated the super folding element (SFE) theory to describe the relationships between deformation mechanisms and energy absorption criteria. Their study has facilitated the development of thin-walled metallic structures that have found wide applicability in safety designs over the decades. Based on the premise that mechanisms for the dissipation of kinetic energy in crash situations in high-speed transportation can easily follow a predictable and controllable scenario, tailorable aluminum composites have evolved for best performances. However, one of the major constraints associated with the arbitrary incorporation of metallic structures is the density effect, because it is somewhat

challenging to have a lightweight absorber with a correspondingly high specific energy absorption (SEA) index which is the major requirement in many applications [2]. To circumvent this limitation in view of the sophisticated requirements for safety in modern transportation, the quest for light-weight structures in certain automotive applications continues to expand with growing interest in fiber-reinforced composites [2]. To this end, hybrid composites and other carefully-engineered, synthesized material forms are candidates for superior performance in the automotive and aerospace applications.

The hybridization of fibers and metals has been shown to achieve a good compromise in specific strength and modulus for shell structures and thin tubular sections with profound energy absorption performances. For instance, the authors [3] investigated the quasi-static axial crushing behavior of hybrid wrapped glass fibre reinforced polymer (GFRP) and square aluminum tubes in order to evaluate the inference of ply orientations, and they found that the performances of the hybrid tubes were superior to those of the aluminum tubes. The crashworthiness of a vehicle energy absorber has been studied based on a hybrid square hollow steel tube filled with glass-fiber reinforced 'polyamide 66' honeycomb structure [4]. Furthermore, to address the scenarios of oblique collisions in crashes, the authors investigated the ultimate bending moments and energy-absorption performance of aluminum/GFRP hybrid tube beams with emphasis on the effects of thin GFRP skin layer in relation to bending deformation behavior and fracture characteristics and they found the optimal thickness and layup of the composite skin layer consistent with the best performance of the hybrid tubes [5]. Metal-hybrids with synthetic fibers have also been achieved for strategic purposes. The effect of geometry and energy absorption of square cross section, graphite/epoxy and Kevlar/epoxy tubes under static crushing has been investigated in which the effect of decreasing width-wall thickness (b/t) ratio was correlated with increasing energy absorption [6].

As the requirements for energy absorption performance have heightened particularly in motorsport applications where fiber-reinforced polymers are often the primal choice, the prohibitive costs of synthetic fibres (carbon-fibre, kevlar, aramid, etc.,) along with growing environmental concerns on recyclability, has inspired the need for technologically-viable alternatives. In this purview, incorporating natural fibres as second phase materials in developing hybrid composites has indicated promising and desirable results [7]. Some natural fibers such as jute, hemp, sisal, kenaf, coir, flax, banana etc., have been shown to exhibit mechanical properties comparable to glass fibers [7]. This quality, coupled with their low densities, biodegradability, renewability, availability and low costs, make them directly applicable in lightweight, cost-effective automotive applications. Therefore, in line with the requirements of crash safety, hybrid natural fibre based composites have been investigated on their impact performances. For instance, the authors [8] have documented that a hybrid composite laminate of banana/E-glass fabrics reinforced polyester could possess a considerable impact resistance; also a hybridization mechanism to enhance the impact strength of jute/glass and jute/carbon-reinforced composites has been postulated [8], similarly, the post-impact behavior and damage tolerance capability of hemp-based fiber-reinforced polymers have been studied to determine the hybridization effect of basalt fiber additions [8].

The hybridization concept is very significant in improving the overall performance of composites and on this premise, this study focuses on investigating the hybridization effect of the inexpensive, naturally-occurring coir-fibres with high strength aluminum alloy 6063 taking into consideration variations in the concentrations of the coir-fibre and thickness of cylindrical aluminum tubes towards developing an efficient, low-cost, high-performance energy absorbing structures.

2. Materials and Methods

2.1 Composite material specifications

The hybrid composite structure consists of a primary (natural coir fibre) and secondary aluminum alloy 6063 in combination with an epoxy-resin matrix. The coir-fibre is a biodegradable natural lignocellulosic filler and the aluminum alloy (AA 6063) is an age-hardenable alloy with excellent dynamic deformation characteristics. The physical properties of the coir fibre, aluminum alloy and epoxy resin (LY556) are shown in Table 1.

Table 1. Baseline physical properties of coir fibre, AA 6063 and epoxy

Material	Tensile strength (MPa)	Young's modulus (GPa)	Elongation at break (%)	Density (g/cm^3)
Coir fibre [30]	220	6	15-25	1.25
AA 6063	145-186	68.3	18-33	2.69
Epoxy	31	3.7	-	1.15

2.2 Material constitutive modelling

The coir-fiber is constituted by continuous fibres with high aspect ratio, corresponding to infinitely large length-to-diameter (L/D) ratio, an approximation consistent for stiff and strong fibers. The failure initiation of the hybrid composite can be described according to the Hashin's damage law when any of the following four failure modes of fiber tension (F_t), fibre compression (F_c), matrix tension (F_{mt}) and matrix compression (F_{mc}) has a value that is equal or greater than unity.

$$F_t = \left[\frac{\widehat{\sigma_{11}}}{X_T}\right]^2 + \left[\frac{\widehat{\sigma_{12}}}{S_L}\right]^2 = 1 \tag{1}$$

$$F_C = \left[\frac{\widehat{\sigma_{11}}}{X_C}\right]^2 = 1 \tag{2}$$

$$F_{tm} = \left[\frac{\widehat{\sigma_{22}}}{Y_T}\right]^2 + \left[\frac{\widehat{\sigma_{12}}}{S_L}\right]^2 = 1 \tag{3}$$

$$F_{cm} = \left[\frac{\widehat{\sigma_{22}}}{2S_T}\right]^2 + \left(\left[\frac{Y_c}{2S_T}\right]^2 - 1\right)\left[\frac{\widehat{\sigma_{22}}}{Y_C}\right]^2 + \left[\frac{\widehat{\sigma_{12}}}{S_L}\right]^2 = 1 \tag{4}$$

Where $\widehat{\sigma_{11}}$ and $\widehat{\sigma_{22}}$ are the effective stress tensor components, X_T and X_C, are the fibre tensile and fibre compressive stresses; Y_T, and Y_C are the matrix tensile and matrix compressive stresses; while S_L and S_T are the longitudinal and transverse shear strengths respectively. The constitutive equations for interlaminar failure is of the form Eq. 5.

$$\sigma = C_{dm}\varepsilon \tag{5}$$

Where σ, ε are the stress and strain components respectively. The C_{dm} is the stiffness matrix indicating damage which is further expressed according to the elastic constants by;

$$C_{dm} = \frac{1}{D}\begin{bmatrix} (1-d_f)E_{11} & (1-d_f)(1-d_m)v_{21}E_{11} & 0 \\ (1-d_f)(1-d_m)v_{12}E_{22} & (1-d_m)E_{22} & 0 \\ 0 & 0 & D(1-d_s)G_{12} \end{bmatrix} \tag{6}$$

Where the damage variables for tension, compression and shear are given by d_f, d_m and d_s respectively. The scalar damage parameter D is associated with plastic strain and defines the degradation of material stiffness according to the expression;

$$\boldsymbol{D} = 1 - (1 - d_f)(1 - d_m)v_{12}v_{21} \tag{7}$$

Delamination between coir fibres and epoxy resin is analyzed by the cohesive zone (CZM) model approach according to the quadratic loss function or traction-separation criterion;

$$\left\{\frac{\langle\tau_n\rangle}{\tau_n^0}\right\}^2 + \left\{\frac{\langle\tau_s\rangle}{\tau_s^0}\right\}^2 + \left\{\frac{\langle\tau_t\rangle}{\tau_t^0}\right\}^2 = 1 \tag{8}$$

Where, t_n^0, t_s^0, t_t^0 are the peak values of the nominal stress components across the interface. The failure initiation displacements U_n^0, and U_s^0, can be expressed as follows:

$$U_n^0 = {\sigma_n}/{E_p}; \qquad U_s^0 = {\sigma_s}/{E_p} \tag{9}$$

Where, σ_n, σ_s, E_p, are the normal compressive strength, shear strengths and stiffness at the interface respectively. The final displacements U_n^1 and U_s^1 are obtained from the fracture toughness G_n for the normal mode and critical energy release G_s for the shear mode according to the relations:

$$U_n^1 = {2G_n}/{\sigma_n} \qquad U_s^1 = {2G_s}/{\sigma_s} \tag{10}$$

The effective separation displacement for the normal and shear separations is determined using;

$$\delta_m = \sqrt{\delta_n^2 + \delta_s^2} \tag{11}$$

The mixed-mode damage initiation criteria can then be expressed by;

$$\delta_m^0 = U_n^0 \times U_s^0 \times \sqrt{\frac{1 + \beta^2}{U^{0^2}_s + (\beta \times U_n^0)^2}} \tag{12}$$

Where $\beta = \frac{U_s}{U_n}$, the total separation by mixed-mode failure is then obtained through the Benzeggagh-Kenane (B-K) criterion with γ is the (B-K) criterion exponent relations;

$$\delta_m^f = \frac{2}{E_p \times \delta_m^0}[G_n + (G_s - G_n)] \times \left(\frac{\beta^2}{1 + \beta^2}\right)^\gamma \tag{13}$$

The damage evolution variable $\boldsymbol{D}$ is expressed in terms of the maximum mixed-mode δ_{max}, by

$$D = \frac{\delta_m^f \times (\delta_{max} - \delta_m^0)}{\delta_{max} \times (\delta_m^f - \delta_m^0)} \tag{14}$$

2.3 Numerical implementation

2.3.1 RVE homogenization

To simulate composite structures, effective material properties are required, and in most cases, these properties are difficult to measure prompting the need for numerical homogenization. The elastic properties and strength parameters of coir fibre/epoxy are required for the Hashin's progressive damage model and analysis of the hybrid composite, but since this is not readily available in the open literature it was found by implementing the Mori-Tanaka/Eshelby mean field model as a homogenization scheme in DIGIMAT 2017.0 software. In this special case, the elastic moduli viz; longitudinal modulus E_{11}, transverse modulus E_{22}, longitudinal shear modulus G_{12} , transverse shear modulus G_{23} and major Poisson's ratio v_{12}, were determined. The governing mathematical formulation of Mori-Tanaka and Benveniste [9] are given by the following relations that express the stress in the reinforcing fibres and the matrix by Eq. 15 and Eq. 16 respectively.

$$\sigma_f = \sigma_m + C_m\left(e^0 + e_f^C - e_f^T\right) + C_m\left(\bar{e} + e_f^C - e_f^T\right) \tag{15}$$

$$\sigma_m = \sigma_0 + C_m\bar{e} = C_me^0 + C_m\bar{e} \tag{16}$$

Where, σ_0 is the external stress applied to the composite, C_m, e^0 and $\bar{e}$ are the stiffness tensor, the mean strain of the matrix and the eigenstrain or disturbance strain in the matrix due to the fibers. The constrained strain in the fibres and the mismatch strain between the matrix and the fibres are given e_f^C and e_f^T respectively. The stiffness tensor of the composite C_s is expressed via the relations;

$$C_s^{-1} = [I + fB(I + Q)]C_m^{-1} \tag{17}$$

Where, $B = \left(\left(C_f - C_m\right)S + C_m^{-1}\right)\left(C_f - C_m\right); \quad Q = (I + f(S - I)B)^{-1}(-f(S - I)B) \tag{18}$

C_f, f, S and I are the stiffness tensor of fiber, fiber volume fraction, Eshelby tensor and identity tensor, respectively. In DIGIMAT 2017.0, the boundary value problem on the RVE of the epoxy/coir fiber composite (Fig. 1) is solved by substituting the elastic modulus and Poisson's ratio of the epoxy matrix and coir fibres into Eq. 17, to generate a homogenized and stress-strain response which determines the effective elastic moduli of the composite.
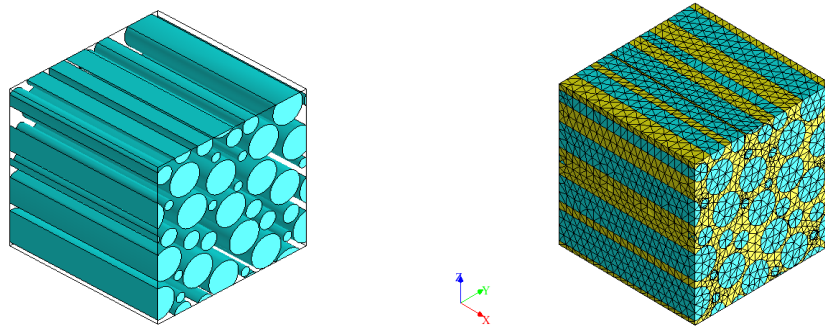

Fig. 1. Representative volume element (a) fibre-matrix   (b) meshed structure.

2.3.2 Structural modelling

Numerical analysis was performed using ABAQUS/Explicit [41] to predict the load-deformation behavior and stress-contour profiles of the tubes, incorporating the interlaminar damage initiation and evolution criteria. The model as shown in Fig. 2, consists of a rigid top and bottom plates in counter-acting positions with the deformable coir-fibre/aluminum structure. The motion of the top plate is restricted to an axial vertical direction while the bottom plate is fixed. To prevent the initial penetration of the top plate and the deformable structure, a minimum clearance 0f 0.001mm was applied between the assemblies. A tangential behavior, 'surface-to-surface' contact condition was used to describe the interacting contacting surfaces with a penalty frictional formulation of 0.2. The top surface of the rigid bottom plate and the bottom face of the deformable structure are coupled by the 'node-to-surface' interaction criterion and the lateral motion of the contact was prevented by the 'rough' frictional contact condition. The top plate and rigid bottom were discretized with the 4-node 3D bilinear quadrilateral element 'R3D4' with an element size of 4.8mm. The deformable structure was discretized by the shell element 'S4R' with three integration points. The material properties for the homogenized coir-fiber/epoxy systems were incorporated to the deformable shell structure using the composite lay-up function. Axial load of *100N* was imposed from the top plate with a velocity of 15.6 m/s. The effective crushing distance is set at 20mm which is about 67% of the total length of the overall assembly.
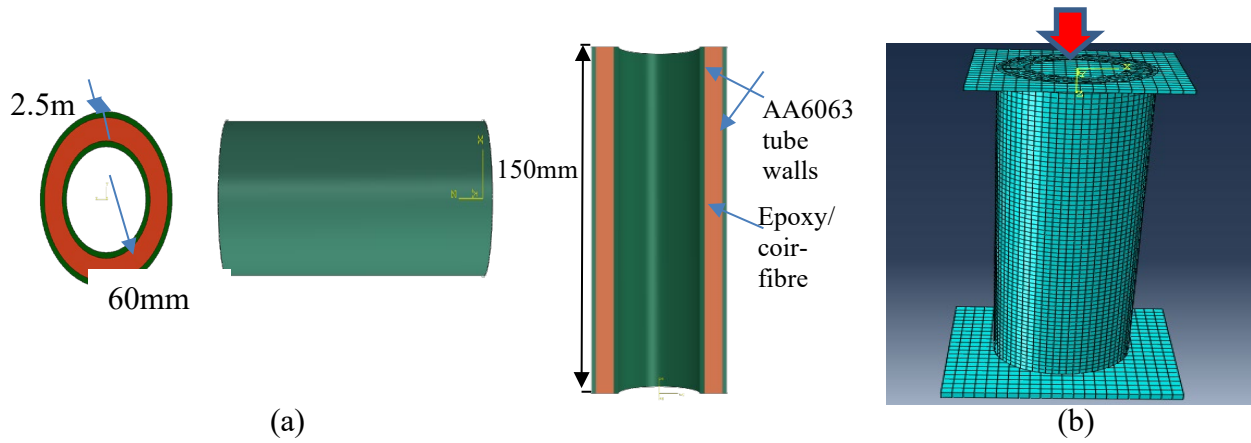
Fig.2. (a) Geometry of aluminum/coir-fibre tubes (b) meshed geometry

3. Results and Discussions

3.1 Deformation profiles of composite tubes

The load-displacement curves in Fig. 3 describe the coupled elastic-plastic response based on the von Mises J_2 plasticity, and the damage initiation to evolution behavior of Hashin. The stress-strain plots suggest that a resistance to crush loads is much higher for the 20T samples over a wide range of displacement as compared with the 10T samples, and the variations from axisymmetric (high resistance to large deformation) to non-axisymmetric (low resistance to crushing) response is also less significant. Also, the period of dynamic progressive crushing is much longer which is an evidence of a strong interaction between the tube walls and reinforcements in preventing the formation of complete folds. On the other hand, the fluctuations in crushing loads is less significant for the 10T samples probably due to a low frequency of local buckling, but in general the period of progressive crushing is much limited and this could be attributed to accelerated sequence of complete fold formations. Concerning the 15T tubes, the onset of unstable buckling load response of the tube-wall probably led to non-uniform folds and plastic instability at the beginning of the crushing process based on the inherent fluctuations in the elastic region, nonetheless, the formation of inward and outward folds occurred over a much more elongated period of time as indicated by the smoother load fluctuations which is an evidence of a superior elastic-plastic deformation behavior under progressive crushing due to a stronger frictional resistance interaction between successive folds [1,3]. Also, at the densification stage where the extensional mode of deformation is dominant, there is an evidence of continuous in-plane deformation due to a rise in axial loads, hence by comparing the area under the load-displacement curves for the extensional mode of deformation, the 20T and 15T samples were found to possess the best capacities for energy absorption. Concerning the effects of reinforcement phase, optimal energy absorption performance lies between 40-70% volume concentrations for the 20T specimens, due to the fact that there were more gentle peaks with stable crest and troughs events in the 20T samples indicating a continuous inward and outward folding of the tubes with a potential mixed mode of failure delaying the transformation to global bending to indicate a better capacity for buckling resistance.
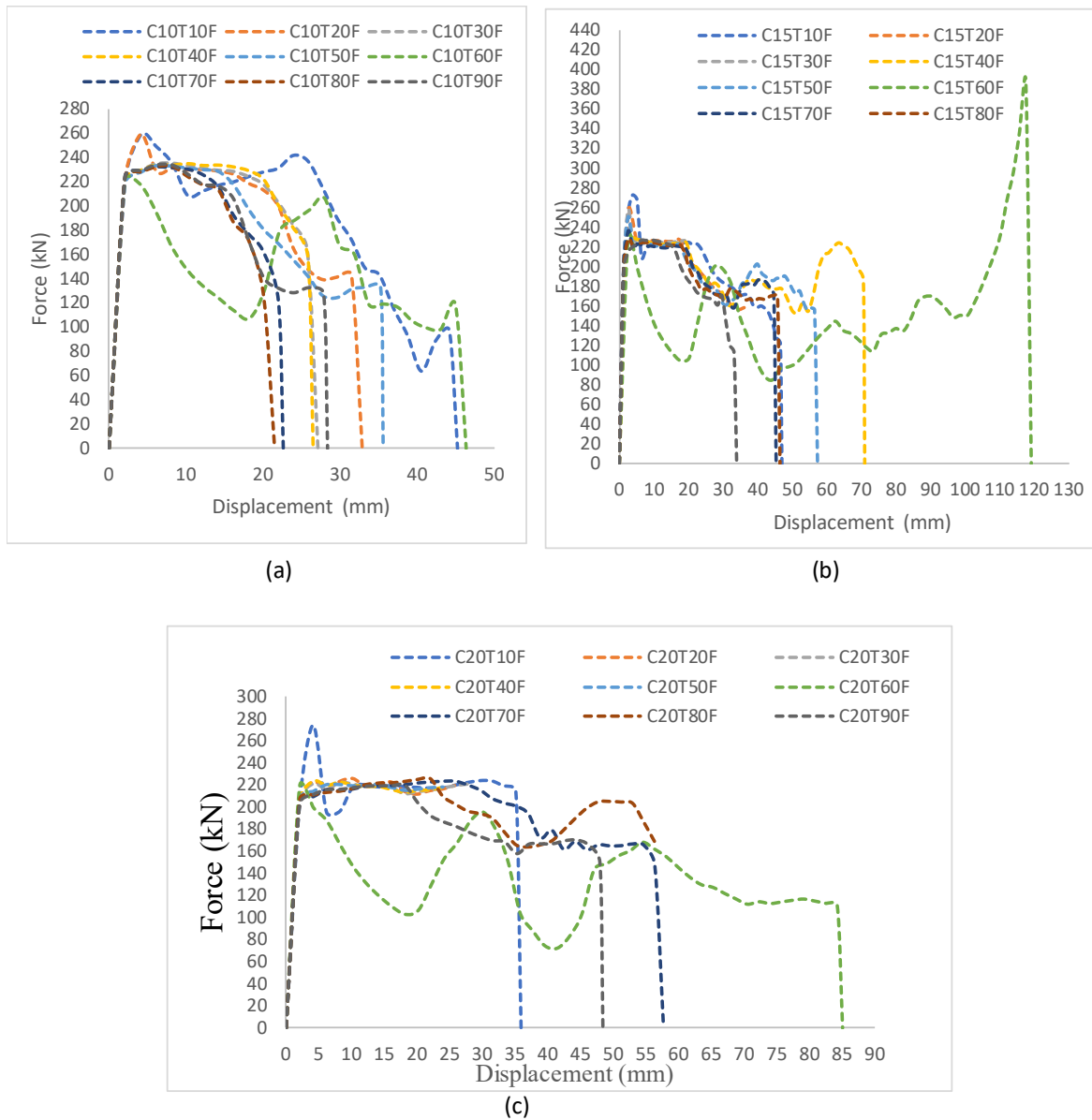
(a)

(b)

(c)

*Fig.3. Graphical representations of the deformation profile of (a) 10T (b) 15T (c) 20T composite tubes*

3.2 Deformation and damage modes of composite tubes

The results of the simulation of the entire structure of the composite incorporating the aluminum matrix, represented by the snapshots of the stress contour plots at varying displacements indicating the damage modes are presented for the damage history of the 10T, 15T and 20T tubes in Figs. 4-6 respectively. Generally, the mechanism of energy absorption is similar for all the configurations and it is characterized by a stable deformation profile and progressive folding effects. As the axial force is applied on the tube by the top plate, the stress wave pattern varies from top to bottom in a quasi-linear manner, and the tube elastically deform under this load until a maximum stress value is attained at the top of the tube. Beyond this point and with the continuous application of load, the tube undergoes plastic deformation and a fold at the top of the tube appears due to the effects of dynamic progressive buckling. From this point, a transformation in the deformation mode of the tube from progressive buckling to bending mode begins, this is accompanied by a decrease in the stiffness of the tube and successive folding of the tube. As the load decreases further due to plastic

deformation, successive folds come together in intimate contact and start to collapse into other folds instantaneously in what could be described as a plastic buckling mode [2, 5]. It is observed that the fiber-reinforced tubes undergo a circumferential breakage due to the successive internal-external bending of the tube walls. The compressive forces introduce bending strains at the contact surface of impact causing matrix and fibre failures [1]. In correlation with Fig. 3 (a), (b) and (c). it is reasonable to suggest that the failure modes of the 20T tubes were more complex
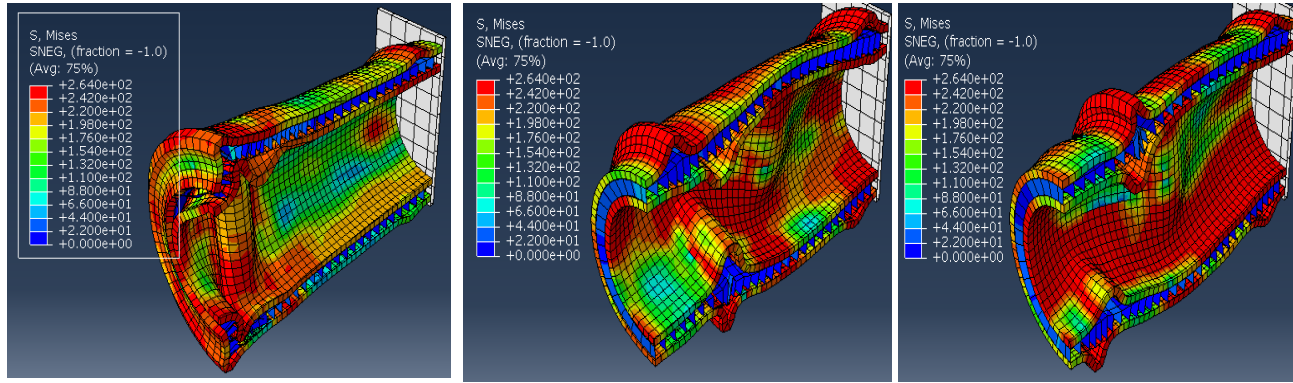
(a)   (b)   (c)

Fig.4. Deformation profile for the 10T composite tubes at (a) 10% (b) 60% (c) 90% volume fraction of coir-fibre reinforcements
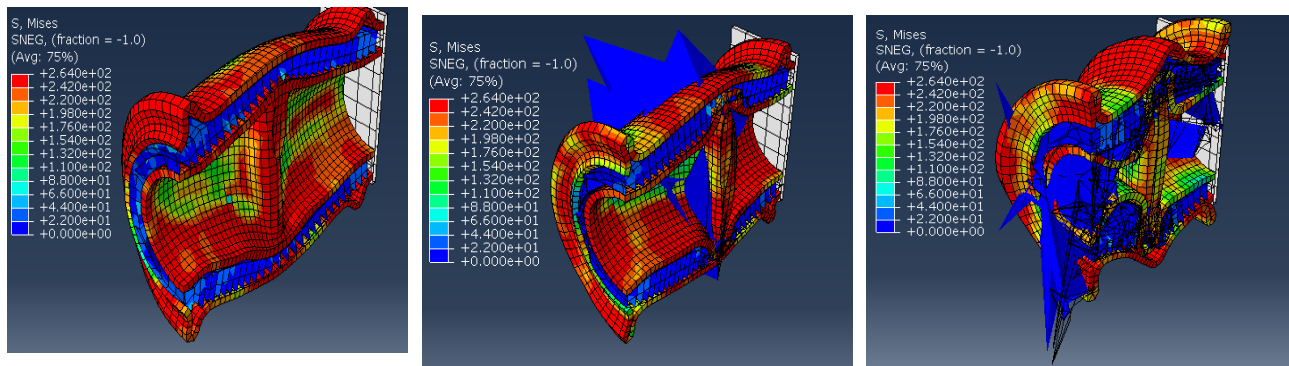
(a)   (b)   (c)

Fig.5. Deformation profile for the 15T composite tubes at (a) 10% (b) 60% (c) 90% volume fraction of coir-fibre reinforcements
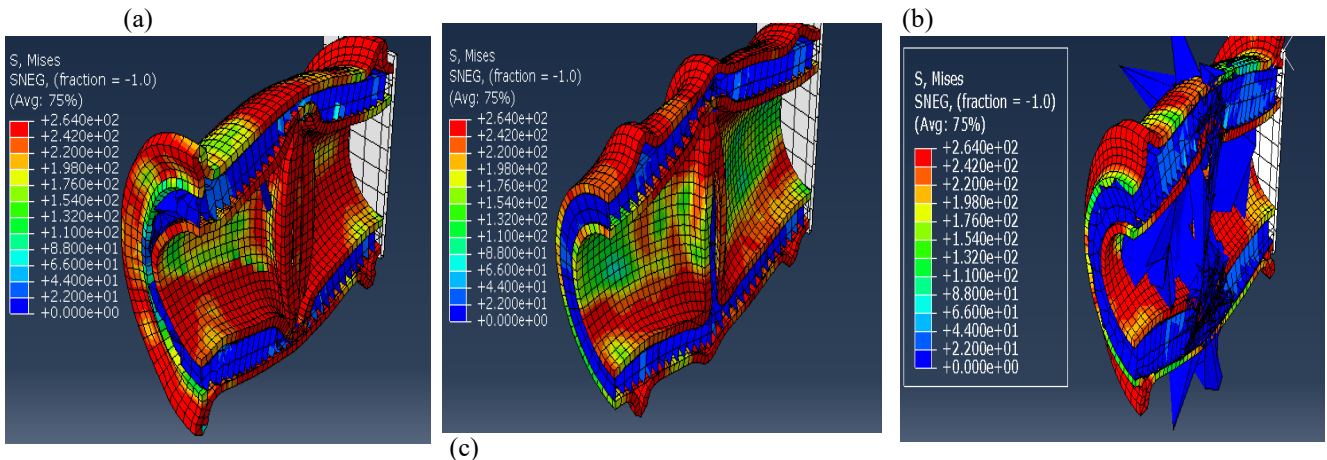
(a)   (b)

(c)

Fig.6. Deformation profile for the 20T composite tubes at (a) 10% (b) 60% (c) 90% volume fraction of coir-fibre reinforcements

because the initial peaks were high due to high stiffness of the tubes, also a gradual reduction in peak forces after the plateau deformation region can be readily observed indicating a propensity for significant energy absorption through extensional collapse modes with progressive delamination damage. For the 10T samples the range of best performance lies within 30-60% samples by virtue of the progressive patterns of the associated curves, but for the 10-20% samples, the effect of stiffness degradation is responsible for their limited crushing distance to the collapse of the tube walls translating to an inferior energy absorption performance, while for the 80-90% reinforced samples, the effect of accumulated matrix damage indicated by their non-linear responses retarded their energy absorption performances at the self-contact stage. For the 15T samples, the onset of matrix damage is prominent for 10-30% as indicated by their non-linear response, but the range of best performance is between samples with 40%-70% volume fraction of reinforcement where associated family of curves indicated steady fluctuating patterns probably due to the effects of a more progressive crack propagation events occurring along the longitudinal axes of the tubes during compression that consequently introduced a transitional mode of deformation through progressive delamination damage. Lastly, concerning the response of the composite models at high volume fractions (80-90%), the onset of early densification can be attributed to the influence of the dense fibre content in accelerating matrix damage, causing a detachment of the fibres from the matrix, even though the capacity to absorb more loads was still retained [5]. Hence, for optimal design performance, it may be impracticable to incorporate high-volume fraction of coir-fibres by the hybridization concept.

3.3 Experimental validations
Quasi-static experiments were conducted on 10T, 15T and 20T tubes constituted with 60% coir-fibre content and the results as presented in Fig. 7 showed that the deformation profiles were
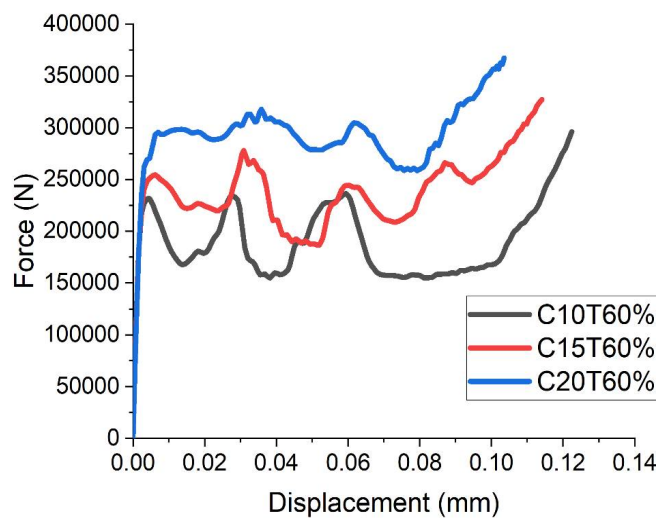
Fig.7. Experimental validation (a) stress-strain plots (b) composite tubes (c) cross-section of tube

consistent with simulated performance indicating a relatively wider range of progressive crushing of the 20T reinforced tubes to underscore its superior energy absorption capacity.

Conclusions

1. The mechanism of deformation and damage was similar for the tubes at 10-30% reinforcement concentration characterized by circumferential fiber breakage and matrix damage while at 80-90%, unsteady non-linear response by global bending degraded the tubes' resistance to buckling. The elongated plateau regions of the tubes at 40%-70% indicate the range of best performance.

2. The resistance to formation of complete folds increased significantly with the evolution of reinforcement thickness where-in the 20T tubes indicated complex profiles after initial peak stresses that constrained axisymmetric to global bending transformations.

3. The 20T tubes were found to demonstrate the best energy absorption performance due to a superior resistance to buckling occasioned by a stable dynamic progression during crushing and by controlled delamination damage under extensional collapse during densification.

4. The results on the performance of the tubes were consistent with experimental observations.

References

[1] Weirzbicki, T and Abramowicz, W (1983). On the crushing mechanism of thin-walled structures. Journal of applied mechanics, 50 (4), 727-734. https://doi.org/10.1115/1.3167137

[2] Wang, Z., Jin, X., Li, Q and Sun, G (2020). On crashworthiness design of hybrid metal-composite structures, Int. J. of Mechanical Sciences, 171, 105380, Elsevier Science Ltd. https://doi.org/10.1016/j.ijmecsci.2019.105380

[3] Cui, Z., Liu, Q., Sun,Y and Li, Q (2020). On crushing responses of filament winding CFRP/aluminum and GFRP/CFRP/aluminum hybrid structures, Composites Part B: Engineering, 200, 108341, Elsevier Science Ltd. https://doi.org/10.1016/j.compositesb.2020.108341

[4] Paz, J., Diaz, J., Romera, L and Costas, M (2014). Crushing analysis and multi-objective crashworthiness optimization of GFRP honeycomb-filled energy absorption devices, Finite Elements in Analysis and Design 91, 30-39, Elsevier Science Ltd. https://doi.org/10.1016/j.finel.2014.07.006

[5] Jung, D., Kim, H and Choi, N (2009). Aluminum-GFRP hybrid square tube beam reinforced by a thin composite skin layer, Composites Part A: Applied Science and Manufacturing, 40 (10), 1558-1565, Elsevier Science Ltd. https://doi.org/10.1016/j.compositesa.2009.06.015

[6] Farley, G (2016). Effect of specimen geometry on the energy absorption capability of composite materials, Journal of Composite Materials, 20 (4), Sage Journals. https://doi.org/10.1177/002199838602000406

[7] Islam, M; Hasbullah, N; Hasan, M; Tahb, Z; Jawaid, M and Haafiz, M (2015). Physical, mechanical and bio-degradable properties of kenaf/coin hybrid fiber reinforced polymer nanocomposites. Materials Today Communication, 4, 69-76. https://doi.org/10.1016/j.mtcomm.2015.05.001

[8] Jawaid, M; Thariq, M and Saba, N (2019). Mechanical and physical testing of bio-composites, fiber-reinforced composite and hybrid composites wood herd publishing, Elsevier, 43-57.

[9] Benveniste, Y (1987). A new approach to the application of Mori-Tanaka's theory in composite materials. Mechanics of materials 6 (2): 147-157. Elsevier Science Ltd. https://doi.org/10.1016/0167-6636(87)90005-6